

Visual Identification of Articulated Object Parts

Vicky Zeng¹, Tabitha Edith Lee^{2†}, Jacky Liang^{3†}, Oliver Kroemer⁴

Abstract—As autonomous robots interact and navigate around real-world environments such as homes, it is useful to reliably identify and manipulate articulated objects, such as doors and cabinets. Many prior works in object articulation identification require manipulation of the object, either by the robot or a human. While recent works have addressed predicting articulation types from visual observations alone, they often assume prior knowledge of category-level kinematic motion models or sequence of observations where the articulated parts are moving according to their kinematic constraints. In this work, we propose training a neural network through large-scale domain randomization to identify the articulation type of object parts from a single image observation. Training data is generated via photorealistic rendering in simulation. Our proposed model predicts motion residual flows of object parts, and these residuals are used to determine the articulation type and parameters. We train the network on six object categories with 149 objects and 100K rendered images, achieving an accuracy of 82.5%. Experiments show our method generalizes to novel object categories in simulation and can be applied to real-world images without fine-tuning.

I. INTRODUCTION

Reliable, autonomous robots have many potential applications as assistants to humans in settings such as homes, businesses, and hospitals [1]–[6]. One prerequisite for these applications is the capability for robots to both recognize and manipulate **articulated** objects: objects that have moving parts that are kinematically linked with each other, such as doors, windows, drawers, caps, dials, buttons, and switches. For example, a robot tasked with fetching medicine must identify and interact with several articulated objects: opening a door to enter a room, searching a cabinet of drawers for a medicine bottle, twisting the bottle cap open, and then delivering the contents. Manually specifying articulation constraints for a large variety of objects is intractable, so it is important for a robot to autonomously identify these constraints and their parameters.

Interactive Perception (IP) is a well-known approach to this problem [7]. With IP, the robot actively interacts with objects in the environment through physical contact, observes the changes, and makes predictions about what kinematic constraints might be present. For example, the robot may pull on a handle, and if the handle’s trajectory forms a straight line, then the constraint is prismatic (e.g., drawer); if the handle follows an arc, then the constraint is revolute (e.g., door). Prior works in IP often share the limitation that



Fig. 1: Predicting articulation mechanism from input images. Given the inputs on the left - RGB image, depth image, and part segmentation masks of two object parts - the model predicts the articulation type between the two parts.

they do not leverage the object’s *visual* features [8]–[11], or leverage visual features only as a contextual prior to exploration [12]. Most articulated objects that humans interact with are designed to signify their articulation affordances through pronounced geometry and texture. An elongated bar with one contact at the end to another surface is probably a revolute handle; a cabinet handle with a connection at each end is likely prismatic.

Another approach is to consider visual aspects while identifying articulation mechanisms. Existing works in this direction track the relative movements of object parts from videos and predict the constraint types [13]–[19]. However, these still require the articulated object to be manipulated in the first place — an onerous assumption for robots interacting with novel environments.

The contribution of our work is a neural network model that identifies articulation mechanisms between objects with only single-frame vision observations, no interactions, and no pre-specified object category model. We leverage recent developments in high-quality object mesh datasets¹ that contain information about both object parts and their relative kinematic constraints. Color and depth (RGB-D) images, as well as part segmentation masks, are collected across six object categories found in PartNet-Mobility [20]. These categories include common household objects like doors, windows, and cabinets. Training images are rendered in simulation with domain randomization. To predict articulation type, we represent and encode the displacement of an object part under a given articulation mechanism as motion

¹Carnegie Mellon University. vzz@andrew.cmu.edu

²Carnegie Mellon University. tabithalee@cmu.edu

³Carnegie Mellon University. jackyliang@cmu.edu

⁴Carnegie Mellon University. okroemer@andrew.cmu.edu

† Equal Contribution

¹<https://sim2realai.github.io/Synthetic-Datasets-of-Objects-Part-I/>

residual flow. The network uses transposed convolutions to predict this flow and the parts’ “connectedness” (i.e., whether two object parts are connected), which we then post-process with RANSAC to form the articulation type prediction. We evaluate the performance of the trained network with ablation studies across multiple object categories, and we also demonstrate that it can predict articulation types of objects in real-world images without further fine-tuning. See supplementary materials at <https://sites.google.com/view/articulated-objects/home>

II. RELATED WORK

Our work relates to two broad classes of vision-based object perception for (1) articulation constraints and (2) pose estimation in manipulation settings.

Visual identification of object articulation constraints. To identify articulation mechanism via visual observations, the authors of [21] manually labeled a large dataset with motion parameters, such as the location and axis of revolute and prismatic joints. They then proposed using motion-driven features and losses to train neural networks that jointly solves for motion-driven part segmentation and motion parameters. Here, motion parameters were encoded as displacement and orientation residuals, corresponding to prismatic and revolute joints. However, this method assumes access to the *complete* point cloud of an object, not a partial or noisy point cloud that would be found with egocentric depth sensors used in most robotic manipulation applications.

Later works relaxed the assumption of complete point clouds, but they leveraged knowledge of a set of predefined articulated object categories and their kinematic models. For example, doors would be one category, and cabinets another. Knowledge of object categories allow these algorithms to fit predefined geometric and kinematic models to the observed visual features, which are often point clouds. For instance, in [22] the authors formed Gaussian mixture models over six predefined kinematic models, and they trained a neural network to predict parameters of the mixture model from single depth images. The parameters include kinematic model parameters for each category, the object’s joint configurations, and geometry parameters (e.g., door length). Training data is generated in simulation, and the authors demonstrated the model’s ability to generalize to novel objects within known categories.

In [23] the authors forgo mixture of Gaussians by proposing the articulation-aware normalized coordinate space hierarchy, a canonical representation for each articulated object category. Within this representation, object scales, orientations, and articulation parameters are normalized, allowing a neural network to directly regress to coordinates in this space. The proposed model uses PointNet++ to process point clouds extracted from depth images, and depth image data for training is also generated in simulation.

The authors of ScrewNet [24] removed the assumption of known object categories or kinematic models. Instead, they represent the relative motion of point clouds as a screw motion: rotation of a body around an axis coupled with a

translation in the axis. ScrewNet is a neural network that directly predicts parameters of this screw motion between articulated parts, inferring articulation type without known kinematic models. However, to make this prediction, the network requires a sequence of depth images, with the articulated object parts moving relative to each other.

Like [24], our work does not require prior definitions of category-level kinematic models. Instead, our proposed method uses a single image observation to perform articulation type; no observations of part motion is required.

Vision-based object pose estimation for manipulation.

Our work can be viewed as a form of vision-based pose estimation, wherein we infer the constrained poses that the connected parts of an object would move under the predicted articulation kinematics. In this view, our work relates to pose estimation in manipulation settings, which includes both objects ([25]–[28]) and robots ([29]–[32]). Of these works, PVNet [27] also regresses to a residual (pointing to object keypoints for pose estimation), whereas our motion residual is used to infer the kinematic constraint. For practical manipulation scenarios, we also note the success of DART [33], a depth-based tracking algorithm for articulated models. Our learning-based model facilitates single-image estimation of articulation motion that generalizes without needing a model specification for novel objects, as DART does. Lastly, our system can be integrated into a vision-based manipulation pipeline, such as the one described in [34]. Instead of object pick-and-place, our approach would facilitate object articulated motion, such as opening cabinets and doors.

III. METHOD

In this section, we describe the proposed neural network model for vision-based identification of articulations of object parts, how its training data is generated, and the representations of the model’s inputs and outputs.

A. Overview

Our approach identifies kinematic constraints between pairs of object parts from stationary visual observation alone. We construct a neural network model that takes as input a single-view RGB-D image and segmentation masks of two distinct object parts. Our work focuses on designing and training this network, so we assume the part segmentation masks are provided from a pre-existing algorithm (e.g., [35]). The neural network provides two outputs for the segmented parts: (1) a parts connectedness classification and (2) the motion residual flow, which is the displacement of the second part relative to the first part if the second part moves under their kinematic constraint. Two parts are connected if they are parts of the same articulated object and are neighbors of one another in the object’s kinematic chain. The joint for two connected parts is classified as revolute, prismatic, or fixed, depending on the predicted motion residual flow. Furthermore, we can apply RANSAC on the predicted motion residual flow to extract articulation parameters for revolute (axis of rotation) and prismatic (direction of movement) joints.

| Dataset | Categories | Objects | Info |
|-----------------------|------------|---------|------|
| RBO [36] | 14 | 14 | Y |
| ShapeNet [37] | 3315 | 220K | N |
| PartNet [38] | 24 | 26.6K | N |
| Shape2Motion [21] | 45 | 2.4K | Y |
| PartNet-Mobility [20] | 46 | 2.3K | Y |

TABLE I: Comparison of 3D Object Dataset. Column **info** represents articulation information (y/n).

| | Door | Window | Faucet | Dishw. | Fridge | Cab. |
|---------|------|--------|--------|--------|--------|------|
| Objects | 30 | 28 | 23 | 30 | 20 | 18 |
| Parts | 92 | 112 | 115 | 92 | 98 | 109 |
| Type | R | P | R | R | R | P.R |

TABLE II: Dataset Statistics. **Objects** shows the number of object models. **Parts** shows the total number of distinct object parts. **Type** lists the type of articulations that exist in that category, where R = revolute and P = prismatic. **Dishw.** stands for Dishwasher, and **Cab.** stands for Cabinet.

By formulating our network inference as querying the articulation type between a pair of object parts, the trained network works with images containing an arbitrary number of articulated objects. Therefore, predefined categorical models or shared coordinate spaces of articulated objects are not needed, since the network does not need to reason about multiple articulation mechanisms belonging to specific object categories. In addition, this formulation also allows our model to generalize to object categories unseen during training. The entire kinematic chain of an articulated object in an image can be recovered by querying the network with all pairs of object parts.

The proposed model is trained via a large dataset of synthetically rendered images of articulated objects. Domain randomization and augmentations are applied to the training images, facilitating a network that is robust and invariant to changes in viewpoint, lighting, textures, occlusions, and object joint configurations. Models of articulated objects came from PartNet-Mobility, from which we filtered and cleaned models to form our training set.

B. Dataset of Articulated Objects

We considered several public datasets of objects with object part information for making our training data, including RBO [36], ShapeNet [37], and PartNet [38]. Table I summarizes the different datasets on number of object categories, number of object models, and whether it contains articulation information between object parts.

To train a generalizable articulation identification model, an object dataset is needed that contains a wide variety of object categories, a large number of diverse objects within each category, and labels of articulation types between connected object parts. The RBO dataset is a collection of 14 objects with 358 RGB-D interaction video sequences. While it provides articulation and part segmentation, the relatively small size makes it inadequate as training data. ShapeNet consists of over 3 million 3D CAD models, of which 220K are classified to 3135 categories. PartNet contains roughly 26K models across 24 object categories with good part

segmentation. While ShapeNet and PartNet are sufficiently large, both datasets lack articulation information.

In recent works, Shape2Motion [37] and PartNet-Mobility [20] have augmented ShapeNet and PartNet to include articulation information. Shape2Motion is large with over 2.4K objects. However, it is not amenable to simulation and rendering: it lacks joint limit information and object textures. PartNet-Mobility does not face such limitations and has our desired properties: the dataset has over 2.4K objects across 46 categories, object textures, and articulation information with joint limits. As such, we use PartNet-Mobility to generate the training data for our articulation prediction model (Table II).

We processed meshes from PartNet-Mobility by 1) choosing categories that displayed strong visual signals for its kinematic constraints and 2) selecting a subset of objects from each chosen category. The six categories chosen were doors, windows, faucets, dishwashers, refrigerators and cabinets. In each category, we choose a representative subset of objects that maintains intra-category variability. In total, 149 objects were selected. We cleaned the selected mesh models by scaling meshes to have realistic sizes and standardizing the orientation of their coordinate frames. The former helps to make rendered images more realistic. For example, we would not want a faucet to be the same size as a refrigerator. The latter ensures that objects of the same categories appear in similar poses when loaded for rendering. Without this step, one door model may be upright when viewed at its canonical pose, but another might be upside down. Lastly, we removed object parts and articulation connections that were too detailed. For example, the interior racks of dishwasher models were ignored in our dataset.

C. Dataset of Articulated Object Images

The network is trained using synthetic data with domain randomization and image augmentation. Data was generated using Nvidia Isaac Sim², a GPU-accelerated robotics simulator that supports photorealistic rendering. Articulated objects were loaded into a clean virtual scene and applied several randomizations, including camera pose, scene lighting, object pose, size, texture, and distractor objects. Figure 2 contains some examples of the rendered RGB images.

To make the trained articulation prediction model generalizable across a wide variety of scenes, we perform domain randomizations to render the synthetic dataset. The camera is positioned randomly within the front upper hemisphere of the object, a region where a robot is likely to be to perform manipulation. Joint configurations of articulated objects are randomized within their joint limits. Object sizes are also randomly scaled between 0.5 and 2.0 during generation. In addition, we randomize object textures and scene lighting. These randomizations accommodate for intra-category variation. While household items have diverse appearances (i.e., the width, color and length of doors might differ), these particular differences do not affect the underlying articulation

²<https://developer.nvidia.com/isaac-sim>



Fig. 2: Example synthetic training images for doors after domain randomization and augmentation. We randomized 1) camera positions, 2) object joint angles, 3) object scales, 4) textures, and brightness. Scenes also had 5) distractor objects that introduced occlusions.

mechanisms. Scaling and changing the visual properties of the objects in the training data makes the model invariant to such details. Lastly, distractor objects consisting of common objects and household items are included to produce natural occlusions of articular object parts.

In total, approximately 100K image scenes were rendered, each including an RGB-D image of resolution 640×480 , an object part segmentation image, and the articulation information of objects in the scene.

In addition to domain randomization, we apply standard image augmentation techniques during training, including geometric transformations such as random rotations, flips, and crops. For RGB images, we perform random visual transformations such as contrast and brightness. We also add realistic noises to depth and segmentation masks to make the trained model more robust. For depth images, we apply additive correlated Gaussian noise and multiplicative gamma noise to simulate realistic depth sensor noise [39]. To add realistic noise to the boundaries of the binary segmentation masks, we apply salt and pepper noise followed by a morphological closing operation.

Each data sample during training is generated with a pair of object parts in a rendered image. We first pick a pair of object parts from the segmentation image. Then, the network input consists of the RGB-D image of the entire scene and two binary segmentation masks of the chosen pair of object parts. The output consists of a binary part-connectedness label of the corresponding pair as well as the motion residual flow of the second part relative to the first part. The motion residual flow is a $W \times H \times 3$ image, where each pixel is only non-zero if it occupies a pixel belonging to the second object part. See Figure 5 for some examples. In these non-zero pixels, the values of each pixel correspond to where the corresponding point on the object part in 3D space would be if the object part is moved by a fixed magnitude following its kinematic constraint with the other part. The direction of the motion is expressed in the camera frame. For fixed joints, the motion residual is 0. For revolute joints, the movement magnitude is 30° . For prismatic joints, the movement magnitude is $0.3M$, where M is the maximum joint movement distance provided by PartNet-Mobility.

D. Network Architecture

The neural network for our approach is an hourglass encoder-decoder architecture similar to the network used for DREAM [31]. As shown in Fig. 3, the network takes as input a stacked image observation of size $640 \times 480 \times 6$, with 4 RGB-D channels and 2 part-segmentation mask channels. The network predicts the motion residual flow as a $640 \times 480 \times 3$ image and binary part-connectedness label.

The image encoder consists of the convolutional layers of VGG19 pretrained on ImageNet [40]. The decoder (upsampling) module has four 2D transpose convolutional layers (stride = 2, padding = 1, output padding = 1), and each layer is followed by a normal 3×3 convolutional layer and ReLU activation layer. The first output head is the part connectedness, consisting of 3 fully connected layers. The second output head for the motion residual flow is composed of 3 convolutional layers (3×3 , stride = 1, padding = 1) with ReLU activations with 64, 32, and 3 channels, respectively. There is no activation layer after the final convolutional layer.

The network is trained with a Cross Entropy loss on part connectedness and a Mean Square Error loss on the motion residual flow. Let $y_n^c \in \{0, 1\}$ and $y_n^f \in \mathbb{R}^{640 \times 480 \times 3}$ respectively denote the binary part-connectedness and motion residual flow of the n th training sample, and \hat{y}_n^c, \hat{y}_n^f be their estimated counterparts produced by the neural network. The weighted loss function on the two outputs is defined as:

$$\mathbf{SE}(y_n^f, \hat{y}_n^f) = \|y_n^f - \hat{y}_n^f\|^2 \quad (1)$$

$$\mathbf{CE}(y_n^c, \hat{y}_n^c) = -y_n^c \log(\hat{y}_n^c) + (1 - y_n^c) \log(1 - \hat{y}_n^c) \quad (2)$$

$$\mathcal{L} = \frac{1}{N} \sum_{n=1}^N w_{se} y_n^c \mathbf{SE}(y_n^f, \hat{y}_n^f) + w_{ce} \mathbf{CE}(y_n^c, \hat{y}_n^c) \quad (3)$$

Note that we only propagate the motion residual squared error loss when the parts are connected. The weights $w_{se} = 0.6$ and $w_{ce} = 0.4$ were chosen after hyperparameter search.

E. Articulation Prediction from Motion Residual Flows

If the network predicts that the two queried object parts are connected, then we process the predicted motion residual flow to estimate the part articulation type and parameters. See Alg. 1 for an overview. First, a plane is fitted on the point cloud of the object part in the input observation. We refer to this as the pre-motion plane. Next, we fit a second plane on the point cloud of the object part, where each point is translated by the predicted motion residual flow. We refer to this as the post-motion plane. Refer to Fig. 4 for examples of revolute and prismatic planes.

For fitting both planes, RANdom Sample Consensus (RANSAC) [41] is used to obtain robust estimations. RANSAC is a sample-based estimation algorithm that is resistant to outliers, which in our case is caused by both the depth and segmentation noises present in the network inputs as well as estimation errors in the network outputs. Further, RANSAC is applicable in our case, because we assume object parts have dominant planar surfaces and are rigid bodies undergoing rigid transforms as a result of kinematic

RGB-D and segmentation images

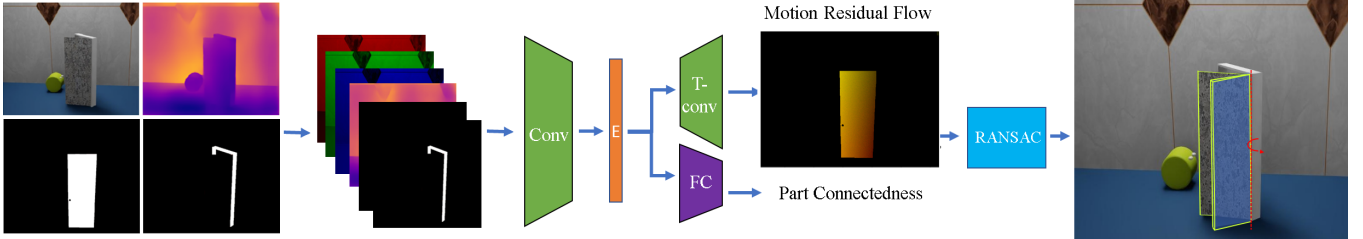


Fig. 3: Neural Network Architecture. The RGB, depth, and segmentation images are stacked into a single network input. Conv means convolution layers, E means intermediate embedding, T-conv means transposed convolution layers, and FC means fully-connected layers. The network produces two outputs: motion residual flow and binary part connectedness. It is post-processed with RANSAC to predict the articulation type.

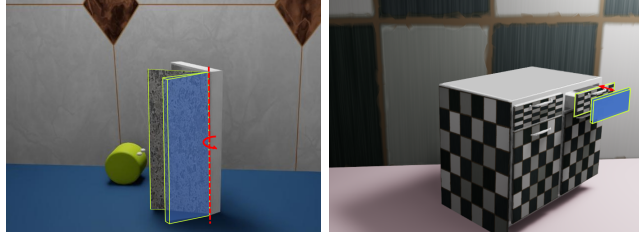


Fig. 4: Visualizations of estimated pre-motion and post-motion planes. In both images, pre-motion planes are outlined in bright green on the original object part, while the post-motion planes are visualized with a blue infill. In the left image, the red annotations denote the estimated axis of the predicted revolute joint. In the right image, the red arrow denote the direction of the prismatic joint.

Algorithm 1 Compute Articulation Type and Parameters from Predicted Motion Residual Flow

Input: Depth image $I_D \in \mathbb{R}^{W \times H}$, binary part segmentation mask $I_S \in \mathbb{Z}_2^{W \times H}$, motion residual flow $I_F \in \mathbb{R}^{W \times H \times 3}$, small thresholds ϵ_0, ϵ_1 .

Output: Articulation Type (AT) $\in \{\text{FIXED}, \text{PRISM}, \text{REV}\}$ and articulation parameters if PRISM or REV.

```

if  $\|I_F\|_2 < \epsilon_0$  then
    return FIXED
end if
Set original point cloud  $P \leftarrow \text{DEPROJECT}(I_D[I_S])$ 
Set estimated displaced point cloud  $P' \leftarrow P + I_F[I_S]$ 
Set pre-motion plane and normals  $\pi, \hat{n} \leftarrow \text{RANSAC}(P)$ 
Set post-motion plane  $\pi', \hat{n}' \leftarrow \text{RANSAC}(P')$ 
if  $\hat{n}^\top \hat{n}' > 1 - \epsilon_1$  then
    Find mean flow  $d \leftarrow \frac{1}{\sum_{w,h} I_S[w,h]} \sum_{w,h} I_F[w, h]$ 
    Normalize into direction  $\hat{d} \leftarrow \frac{d}{\|d\|_2}$ 
    return PRISM,  $\hat{d}$ 
else
    Find intersecting line  $l \leftarrow \text{INTERSECT}(\pi, \pi')$ 
    return REV,  $l$ 
end if

```

constraints. This means that in the noiseless case, the motions of all subsets of points on an object part should be the same.

Comparing the position and orientation of the pre-motion and post-motion planes can give the articulation type and parameters. If the planes are sufficiently close together (the predicted motion residuals are all close to 0), then the predicted articulation type is fixed. Otherwise, if the pre-motion and post-motion planes are sufficiently parallel, then the articulation type is prismatic. In this case, the direction of the prismatic kinematic constraint is the direction of the average motion residual flow. Lastly, if the motion residuals are not all close to 0 and the planes are not parallel, then the predicted articulation type is revolute. In this case, the axis and location of the revolute joint is the line where the pre-motion and post-motion planes intersect. Extracting articulation parameters from motion residual planes in this manner allows the network to learn a single output representation that works for fixed, revolute, and prismatic joints.

IV. EXPERIMENTS

We evaluate our network on synthetic images and show successful transfer to real-world data. Specifically, we report 1) test accuracy achieved with our network with synthetic images when trained on all object categories, 2) generalization to categories unseen during training in a leave-one-out fashion, and 3) generalization to real-world images. An ablation study is further conducted to train the network on each single category and test against all others, to analyze knowledge transfer between categories.

A. Network Training

The neural network was implemented with PyTorch and optimized via the Adam optimizers with a learning rate of 1.2×10^{-4} and momentum of 0.9. These were tuned via hyperparameter search. The training set consisted of 70k images, and the remaining 30k were used in the test set. The network took 30 epochs to train, taking 32 hours on an Nvidia Tesla V100 GPU.

B. Training on All Object Categories

To evaluate the accuracy of the classified articulation types, we separate the predictions into 4 classes: prismatic, revolute, fixed, and unconnected. We refer to this as combined accuracy (CA). Two additional metrics are evaluated:

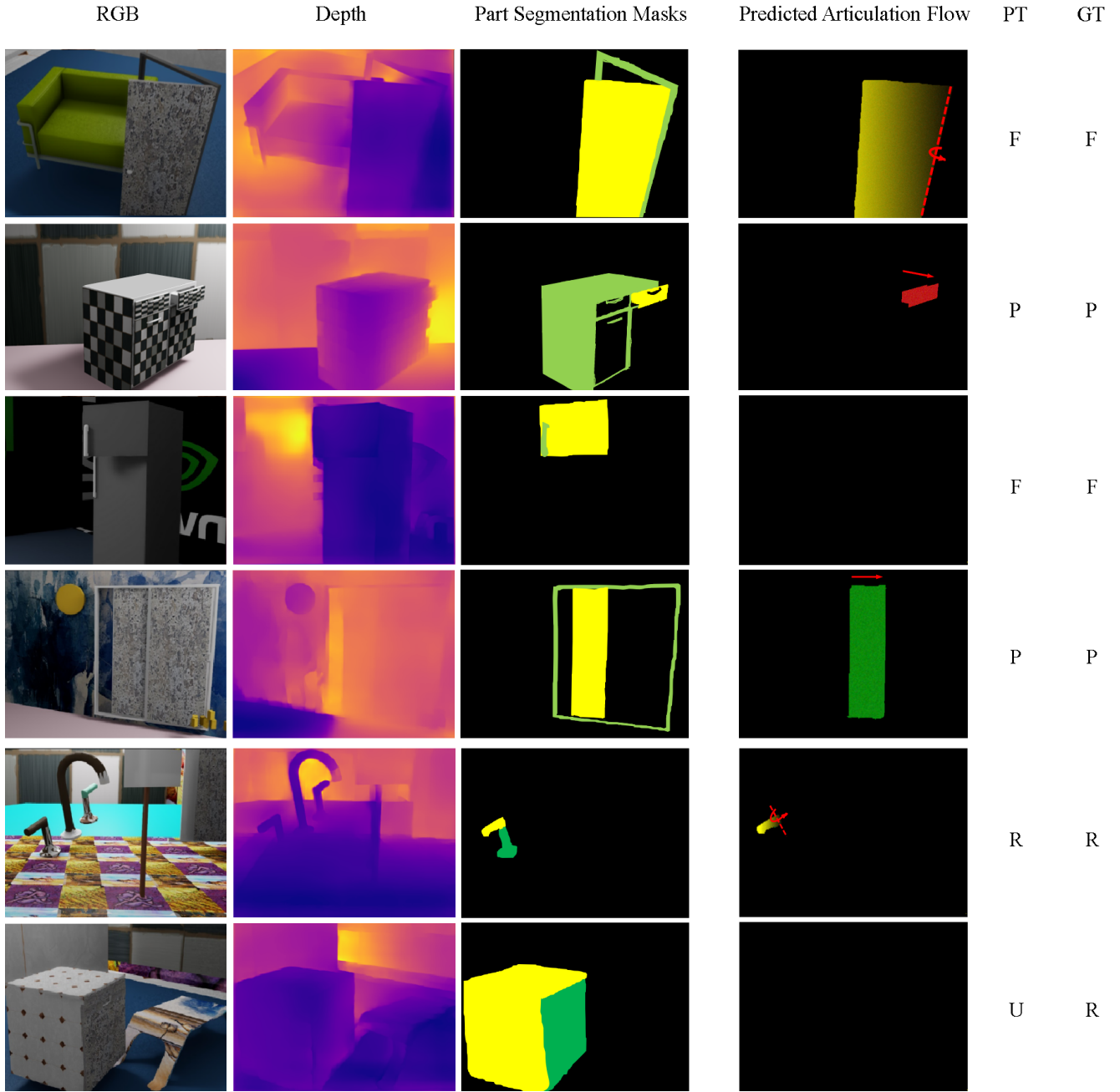


Fig. 5: Visualization of network input-output for each category on synthetic data. PT represents predicted articulation type, and GT represents ground truth type. Articulation is either revolute (R), prismatic (P), fixed (F), or unconnected (U). Network input takes in a stack observation of RGB image, depth image, and two part segmentation masks. The yellow segmentation mask is the anchor object part and the green segmentation mask is the candidate object part. It outputs the predicted articulation flow and part connectedness. We post-process the flow to predict the articulation type. The flow is visualized in the RGB color space, where a prismatic articulation is a single solid color, while a revolute articulation is a gradient towards the axis of rotation. Rightmost column shows the ground truth articulation type. The last row (dishwasher) is an example of incorrect prediction, occurring when visual signal is not observed.

accuracy over part connectedness (**PC**) and accuracy over connected articulation type (**AT**). The former is the binary classification accuracy of whether or not two parts are connected. The latter is only the articulation type accuracy when the network predicts a true positive part connectedness.

Table III shows the test metrics by category when the network is trained on all object categories. Similar test accuracies are achieved across categories.

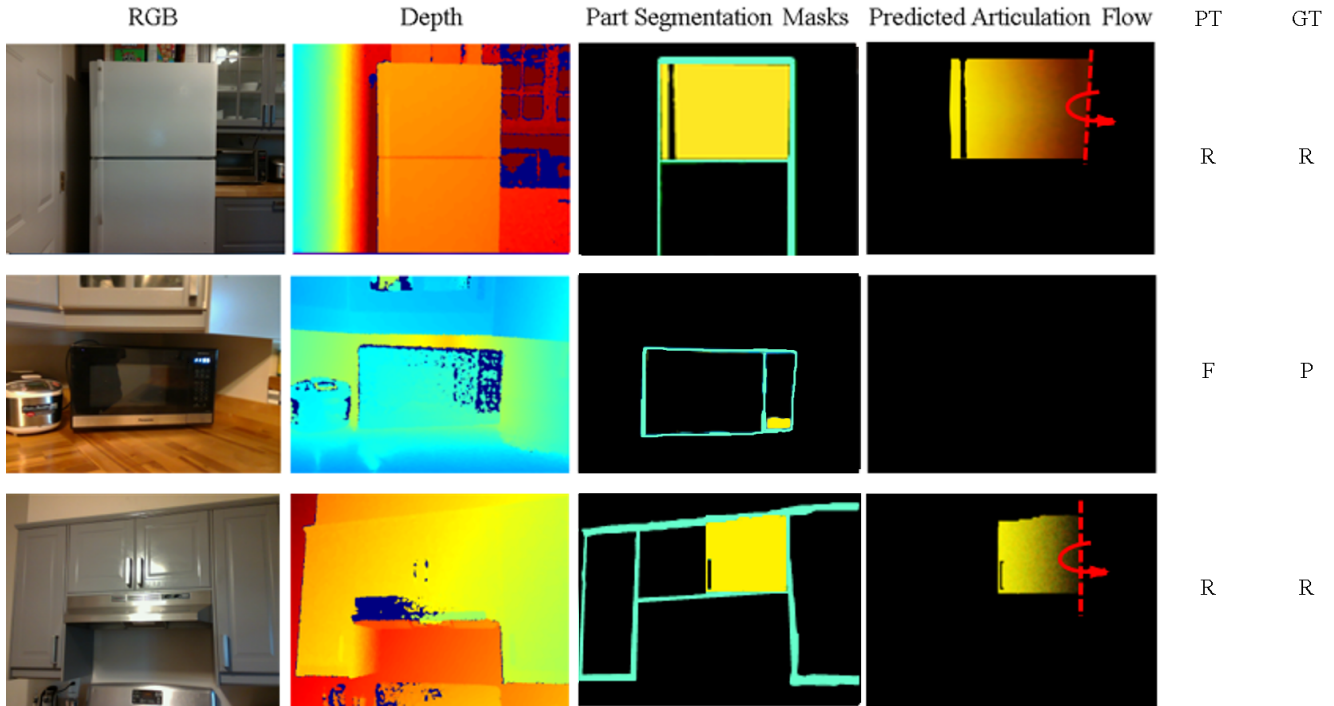


Fig. 6: Visualization of network input-output on real-world images. Network input takes in a stack observation of RGB image, depth image, and two part segmentation masks. It outputs the predicted articulation flow and part connectedness. We post-process the flow to predict the articulation type. See Fig. 5 for more details.

| Metric | Object Category | | | | | | |
|--------|-----------------|-------|-------|-------|-------|------|------|
| | Door | Wind. | Fauc. | Dish. | Frid. | Cab. | Avg. |
| AT (%) | 85.6 | 75.1 | 84.4 | 72.1 | 76.2 | 67.7 | 76.4 |
| PC (%) | 97.8 | 91.2 | 94.6 | 95.7 | 95.4 | 92.5 | 94.1 |
| CA (%) | 88.7 | 79.6 | 87.5 | 78.6 | 84.2 | 77.5 | 82.5 |

TABLE III: Accuracy by Category

C. Generalization to Novel Object Categories

We also evaluate how well the proposed method works when generalizing to novel object categories unseen during training. See Table IV for results. We use a leave-one-out scheme to make this evaluation. Specifically, we train six additional models, with the same hyperparameters, such that each model is trained on all categories except a left out category. Each model is then evaluated on the category it was not trained on.

| Metric | Object Category | | | | | |
|--------|-----------------|--------|--------|--------|--------|---------|
| | Door | Window | Faucet | Dishw. | Fridge | Cabinet |
| AT (%) | 78.8 | 26.5 | 66.2 | 76.3 | 60.3 | 33.5 |
| PC (%) | 94.6 | 96.7 | 85.7 | 95.5 | 93.6 | 89.2 |
| CA (%) | 82.1 | 47.2 | 73.0 | 81.48 | 73.8 | 58.6 |

TABLE IV: Performance on Novel Object Categories.

We observe worst performance on windows and cabinets, mediocre performance on faucets and refrigerators, and best performance on doors and dishwashers. The difference between the best and worst performing category is significant, differing by over 50% for connected parts (windows at 26.5% vs doors at 78.8%). The prediction for windows was worse

than chance.

We investigate the abnormally low AT performance of windows in Table IV, which mainly consists of sliding prismatic joints. High PC across all categories shows that the model identifies connected parts of windows, but it is predicting the wrong articulation types. Analyzing the outputs indicate that most wrong predictions are revolute. We hypothesize two reasons for this: 1) lack of representation of prismatic objects in the training data and 2) misleading revolute objects that share visual similarities with the prismatic windows. Eliminating windows from the training data leaves five categories, of which only one comprises of prismatic-dominant joints.

We also observe similar visual features across windows, doors, and refrigerators, with the latter two as revolute objects. Specifically, they share similar frames, boards and handles, as observed in Fig 7.

High visual similarity between windows and revolute objects in the training set might explain the high prediction rate of revolute for windows. The importance of visual similarity is further reflected in cabinets, the other low-performing category. Although cabinets consist of both prismatic and revolute joints, 73% of the errors occur on the prismatic slots. There was only one training category that was prismatic-dominant, and their object parts showcased conflicting visual features with the cabinets as seen in Fig 8.



Fig. 7: Misleading examples of a window (left) and two doors (right). The shapes of the door panel and window frames, and handles for the window and first door (brown) are similar.

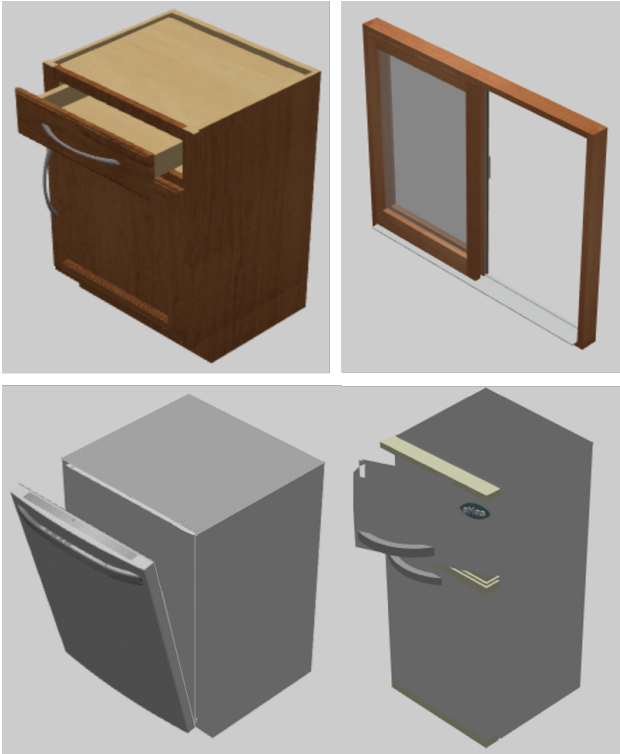


Fig. 8: Misleading examples of a prismatic cabinet (top left) vs other objects (top right prismatic window, bottom revolute dishwasher and refrigerator). The geometry of the cabinet drawer is very different from that of the window, but they both have prismatic joints. By contrast, the handle of the drawer has a similar shape to those of the dishwasher and the refrigerator, even though the latter have revolute joints.

D. Generalization from Training on One Category

We formed hypotheses to explain the low transfer for certain unseen categories in the previous section. A lack of or misleading similarity in visual features of the object parts resulted in misclassifications. This could be significant in our understanding of category generalization. What features and representation do we need in our training categories for good generalization? To answer the question and test our hypotheses, we perform an additional ablation study –

| Train Category | Test Category | | | | | |
|----------------|---------------|--------|--------|--------|--------|------|
| | Door | Window | Faucet | Dishw. | Fridge | Cab. |
| Door | 98.7 | 2.5 | 48.7 | 53.7 | 49.6 | 37.3 |
| Window | 3.2 | 93.2 | 8.9 | 7.8 | 5.6 | 38.2 |
| Faucet | 33.7 | 8.7 | 88.7 | 4.1 | 4.3 | 17.2 |
| Dishw. | 34.2 | 12.8 | 3.8 | 98.5 | 52.1 | 34.6 |
| Fridge | 56.2 | 15.5 | 23.2 | 55.2 | 87.5 | 38.7 |
| Cab. | 49.6 | 32.5 | 13.5 | 3.4 | 38.7 | 83.2 |

TABLE V: Performance of Training on One Category. Overall articulation accuracies when trained on one category (each row) and tested on other categories (each column).

training networks on just a single category and testing them across all the other five categories. See Table V for results.

Learning is limited between articulation mechanisms. Different articulation mechanisms (prismatic, revolute) cannot learn well from each other. When trained on a category with only one articulation mechanism, predicting objects with different articulation is low. For instance, a model trained on windows (prismatic) performs below 10% for all but cabinets (the only other category that contains prismatic joints). We also observe relatively high, consistent performance when testing cabinets, regardless of the trained category. Limited learning between articulation mechanisms explain this better performance because only cabinets contain both articulation mechanisms. Therefore, cabinets have partial representation in each trained category. Consequently, cabinets also fail to achieve at least 40% for any trained category, due to the presence of both articulation mechanisms. Having both articulation mechanisms imply that one of the articulations would be unseen in the train category.

The results also support our hypothesis that misleading similarity in visual features create misclassifications. The lowest transfer occurs between doors and windows. While both performs well on its own category, correct prediction of the other category falls in the 2 – 3% range. Comparing two sample objects from the two categories show similar handles, boards and frames in Fig. 7. However, their ground truth articulation types are different, which explains the low performance. Dishwashers and refrigerators have the highest transfer, and comparing two sample objects show similar handles and physical structure in Fig. 8.

E. Real-world Experiments

Despite only being trained using synthetic data, our network also bridges the reality gap when deployed in the real world. To assess how well our model transfers to real-world data, we took 18 RGB-D images of various household items in our homes (comprising of refrigerators, doors, faucets, and cabinets). Part segmentation masks were generated with semi-automatic DEXTR segmentation [42]. Results showed successful transfers, where the model predicts the correct articulation types for 12 of the 18 images. Example visualizations are shown in Fig 6.

A sample successful example is shown in Fig 6 on the first row. Taking a refrigerator from a clear, front view correctly predicts the revolute joint. An example misclassified image is the microwave on Fig 6 on the second row. The model

predicts no articulation when the correct articulation for the button is prismatic. This is reasonable as most of the kinematic objects in our training data are triggered by knobs, handles or circular buttons, so the model has not seen a microwave button. There is little visual similarity between the microwave button and circular buttons, so low transfer is expected.

V. CONCLUSION

We present a deep learning approach that predicts articulation mechanisms of object parts from a single RGB-D image without physical interactions and pre-specified categorical kinematic models. Training data is generated with a photorealistic robotics simulator with 6 object categories and 149 objects. Domain randomization over camera poses, lighting, object sizes, textures, and occlusions make the trained network robust to these variations. Experiment results show that our approach generalizes to novel object categories in simulation and can be applied to real-world images without fine-tuning.

For future work, we plan to further improve prediction performance by using a wider variety of objects from PartNet-Mobility and other datasets, making the network more robust to misleading visual similarities across object categories, and integrating with interactive perception algorithms.

ACKNOWLEDGMENT

This work is supported by the NSF Graduate Research Fellowship Program Grant No. DGE 1745016, the Office of Naval Research Grant No. N00014-18-1-2775, and the CMU Summer Undergraduate Research Fellowship.

REFERENCES

- [1] J. Bohren, R. B. Rusu, E. G. Jones, E. Marder-Eppstein, C. Pantofaru, M. Wise, L. Mösenlechner, W. Meeussen, and S. Holzer, "Towards Autonomous Robotic Butlers: Lessons Learned with the PR2," in *International Conference on Robotics and Automation (ICRA)*, 2011.
- [2] G. Bekey and J. Yuh, "The Status of Robotics," *IEEE Robotics & Automation Magazine*, vol. 15, no. 1, pp. 80–86, 2008.
- [3] K. Doelling, J. Shin, and D. O. Popa, "Service Robotics for the Home: A State of the Art Review," in *Proceedings of the 7th International Conference on PErvasive Technologies Related to Assistive Environments*, 2014, pp. 1–8.
- [4] P. Dario, E. Guglielmelli, B. Allotta, and M. C. Carrozza, "Robotics for Medical Applications," *IEEE Robotics & Automation Magazine*, vol. 3, no. 3, pp. 44–56, 1996.
- [5] L. D. Riek, "Healthcare Robotics," *Communications of the ACM*, vol. 60, no. 11, pp. 68–78, 2017.
- [6] G.-Z. Yang, B. J. Nelson, R. R. Murphy, H. Choset, H. Christensen, S. H. Collins, P. Dario, K. Goldberg, K. Ikuta, N. Jacobstein, D. Kragic, R. H. Taylor, and M. McNutt, "Combating COVID-19 – The Role of Robotics in Managing Public Health and Infectious Diseases," *Science Robotics*, vol. 5, no. 40, 2020.
- [7] J. Bohg, K. Hausman, B. Sankaran, O. Brock, D. Kragic, S. Schaal, and G. S. Sukhatme, "Interactive Perception: Leveraging Action in Perception and Perception in Action," *IEEE Transactions on Robotics*, vol. 33, no. 6, pp. 1273–1291, 2017.
- [8] J. Sturm, A. Jain, C. Stachniss, C. C. Kemp, and W. Burgard, "Operating Articulated Objects based on Experience," in *2010 IEEE/RSJ International Conference on Intelligent Robots and Systems*. IEEE, 2010, pp. 2739–2744.
- [9] J. Sturm, C. Stachniss, and W. Burgard, "A Probabilistic Framework for Learning Kinematic Models of Articulated Objects," *Journal of Artificial Intelligence Research*, vol. 41, pp. 477–526, 2011.
- [10] S. Höfer, T. Lang, and O. Brock, "Extracting Kinematic Background Knowledge from Interactions Using Task-Sensitive Relational Learning," in *International Conference on Robotics and Automation (ICRA)*. IEEE, 2014.
- [11] P. R. Barragán, L. P. Kaelbling, and T. Lozano-Pérez, "Interactive Bayesian Identification of Kinematic Mechanisms," in *Robotics and Automation (ICRA), 2014 IEEE International Conference on*. IEEE, 2014, pp. 2013–2020.
- [12] C. Moses, M. Noseworthy, L. P. Kaelbling, T. Lozano-Pérez, and N. Roy, "Visual Prediction of Priors for Articulated Object Interaction," *arXiv preprint arXiv:2006.03979*, 2020.
- [13] R. M. Martin and O. Brock, "Online Interactive Perception of Articulated Objects with Multi-Level Recursive Estimation Based on Task-Specific Priors," in *Intelligent Robots and Systems (IROS 2014)*, 2014, pp. 2494–2501.
- [14] D. Katz, A. Orthey, and O. Brock, "Interactive Perception of Articulated Objects," in *Experimental Robotics*. Springer, 2014, pp. 301–315.
- [15] K. Hausman, S. Niekum, S. Osentoski, and G. S. Sukhatme, "Active Articulation Model Estimation through Interactive Perception," in *Robotics and Automation (ICRA), 2015 IEEE International Conference on*. IEEE, 2015, pp. 3305–3312.
- [16] R. Martín-Martín, S. Höfer, and O. Brock, "An Integrated Approach to Visual Perception of Articulated Objects," in *2016 IEEE International Conference on Robotics and Automation (ICRA)*. IEEE, 2016, pp. 5091–5097.
- [17] R. Martín-Martín and O. Brock, "Building Kinematic and Dynamic Models of Articulated Objects with Multi-Modal Interactive Perception," in *AAAI Symposium on Interactive Multi-Sensory Object Perception for Embodied Agents*, AAAI, Ed, 2017.
- [18] M. Baum, M. Bernstein, R. Martín-Martín, S. Höfer, J. Kulick, M. Toussaint, A. Kacelnik, and O. Brock, "Opening a Lockbox through Physical Exploration," in *Humanoid Robotics (Humanoids)*. IEEE, 2017, pp. 461–467.
- [19] C. Eppner, R. Martín-Martín, and O. Brock, "Physics-Based Selection of Informative Actions for Interactive Perception," in *2018 IEEE International Conference on Robotics and Automation (ICRA)*. IEEE, 2018, pp. 7427–7432.
- [20] F. Xiang, Y. Qin, K. Mo, Y. Xia, H. Zhu, F. Liu, M. Liu, H. Jiang, Y. Yuan, H. Wang, et al., "SAPIEN: A SimulAted Part-based Interactive ENvironment," in *Proceedings of the IEEE/CVF Conference on Computer Vision and Pattern Recognition*, 2020, pp. 11 097–11 107.
- [21] X. Wang, B. Zhou, Y. Shi, X. Chen, Q. Zhao, and K. Xu, "Shape2Motion: Joint Analysis of Motion Parts and Attributes from 3D Shapes," in *Proceedings of the IEEE Conference on Computer Vision and Pattern Recognition*, 2019, pp. 8876–8884.
- [22] B. Abbatematteo, S. Tellex, and G. Konidaris, "Learning to Generalize Kinematic Models to Novel Objects," in *Conference on Robot Learning*, 2019, pp. 1289–1299.
- [23] X. Li, H. Wang, L. Yi, L. J. Guibas, A. L. Abbott, and S. Song, "Category-Level Articulated Object Pose Estimation," in *Proceedings of the IEEE/CVF Conference on Computer Vision and Pattern Recognition*, 2020, pp. 3706–3715.
- [24] A. Jain, R. Lioutikov, and S. Niekum, "ScrewNet: Category-Independent Articulation Model Estimation From Depth Images Using Screw Theory," *arXiv preprint arXiv:2008.10518*, 2020.
- [25] J. Tremblay, T. To, B. Sundaralingam, Y. Xiang, D. Fox, and S. Birchfield, "Deep Object Pose Estimation for Semantic Robotic Grasping of Household Objects," in *Conference on Robot Learning (CoRL)*, 2018. [Online]. Available: <https://arxiv.org/abs/1809.10790>
- [26] Y. Xiang, T. Schmidt, V. Narayanan, and D. Fox, "PoseCNN: A Convolutional Neural Network for 6D Object Pose Estimation in Cluttered Scenes," 2018.
- [27] S. Peng, Y. Liu, Q. Huang, X. Zhou, and H. Bao, "PVNet: Pixel-wise Voting Network for 6DoF Pose Estimation," in *Proceedings of the IEEE Conference on Computer Vision and Pattern Recognition*, 2019, pp. 4561–4570.
- [28] P. R. Florence, L. Manuelli, and R. Tedrake, "Dense Object Nets: Learning Dense Visual Object Descriptors By and For Robotic Manipulation," in *Conference on Robot Learning*, 2018.
- [29] J. Bohg, J. Romero, A. Herzog, and S. Schaal, "Robot Arm Pose Estimation through Pixel-Wise Part Classification," in *ICRA*, 2014, pp. 3143–3150.
- [30] F. Widmaier, D. Kappler, S. Schaal, and J. Bohg, "Robot Arm Pose Estimation by Pixel-wise Regression of Joint Angles," in *ICRA*, 2016, pp. 616–623.

- [31] T. E. Lee, J. Tremblay, T. To, J. Cheng, T. Mosier, O. Kroemer, D. Fox, and S. Birchfield, “Camera-to-Robot Pose Estimation from a Single Image,” in *International Conference on Robotics and Automation (ICRA 2020)*, May 2020.
- [32] J. Lu, F. Richter, and M. Yip, “Robust Keypoint Detection and Pose Estimation of Robot Manipulators with Self-Occlusions via Sim-to-Real Transfer,” *arXiv preprint arXiv:2010.08054*, 2020.
- [33] T. Schmidt, R. A. Newcombe, and D. Fox, “DART: Dense Articulated Real-Time Tracking,” *Robotics: Science and Systems (RSS)*, 2014.
- [34] J. Tremblay, S. Tyree, T. Mosier, and S. Birchfield, “Indirect Object-to-Robot Pose Estimation from an External Monocular RGB Camera,” in *Intelligent Robots and Systems (IROS 2020)*, 2020.
- [35] Z. Wang and F. Lu, “VoxSegNet: Volumetric CNNs for Semantic Part Segmentation of 3D Shapes,” *IEEE transactions on visualization and computer graphics*, 2019.
- [36] R. Martín-Martín, C. Eppner, and O. Brock, “The RBO Dataset of Articulated Objects and Interactions,” *The International Journal of Robotics Research*, vol. 38, no. 9, pp. 1013–1019, 2019.
- [37] A. X. Chang, T. Funkhouser, L. Guibas, P. Hanrahan, Q. Huang, Z. Li, S. Savarese, M. Savva, S. Song, H. Su, *et al.*, “ShapeNet: An Information-Rich 3D Model Repository,” *arXiv preprint arXiv:1512.03012*, 2015.
- [38] K. Mo, S. Zhu, A. X. Chang, L. Yi, S. Tripathi, L. J. Guibas, and H. Su, “PartNet: A Large-scale Benchmark for Fine-grained and Hierarchical Part-level 3D Object Understanding,” in *Proceedings of the IEEE Conference on Computer Vision and Pattern Recognition*, 2019, pp. 909–918.
- [39] J. Mahler, J. Liang, S. Niyaz, M. Laskey, R. Doan, X. Liu, J. A. Ojea, and K. Goldberg, “Dex-Net 2.0: Deep Learning to Plan Robust Grasps with Synthetic Point Clouds and Analytic Grasp Metrics,” *arXiv preprint arXiv:1703.09312*, 2017.
- [40] K. Simonyan and A. Zisserman, “Very Deep Convolutional Networks for Large-Scale Image Recognition,” in *3rd International Conference on Learning Representations (ICLR)*, 2015. [Online]. Available: <https://arxiv.org/abs/1409.1556>
- [41] M. A. Fischler and R. C. Bolles, “Random Sample Consensus: A Paradigm for Model Fitting with Applications to Image Analysis and Automated Cartography,” *Communications of the ACM*, vol. 24, no. 6, pp. 381–395, 1981.
- [42] K. Maninis, S. Caelles, J. Pont-Tuset, and L. Van Gool, “Deep Extreme Cut: From Extreme Points to Object Segmentation,” in *Computer Vision and Pattern Recognition (CVPR)*, 2018.